Journal of Solid State Electrochemistry (2024) 28:3163–3173
https://doi.org/10.1007/s10008-024-05879-6

ORIGINAL PAPER

Highly structural stability from small-sized Li_2MnO_3-like domains in Co-free Li-rich layered oxide cathodes

Yu Zhang[1] · Mingxia Yan[1] · Xin Guo[1] · Xu Zhang[1] · Jihong Liu[1] · Shengli An[1] · Guixiao Jia[1]

Received: 3 January 2024 / Revised: 3 March 2024 / Accepted: 27 March 2024 / Published online: 8 April 2024

Abstract

Li-rich layered oxides (LLOs) are attractive cathode materials for high-energy–density lithium-ion batteries. However, the aggregation of Li_2MnO_3-like domains causes critical issues such as capacity/voltage fading and structural transformation. Here, we design the Co-free Li-rich Li-Fe–Ni-Mn–O system with dispersed Li_2MnO_3-like domains (D–LFNMO) and aggregated Li_2MnO_3-like domains (A–LFNMO) to investigate the effect of Li_2MnO_3-like domain sizes on structures and oxidation process using density function theory (DFT) calculations. Structural stability is finished through calculating oxygen release energies and migration energies of Mn^{4+} ions. The oxidation mechanism of oxygen was explored. Uniquely, in the Li-rich Li-Fe–Ni-Mn–O system, O ions in the linear Fe–O-Li configuration are activated to participate into charge compensation. The Fe-doping and especially dispersed Li_2MnO_3-like domains trigger more lattice oxygen ions to avoid the peroxidation of lattice oxygen and suppress the oxygen release. The climbing image nudged elastic band (CI–NEB) calculations find that dispersed Li_2MnO_3-like domains hinder the migration of Mn^{4+} ions to Li-vacancies to form irreversible structures. Consequently, LLOs with dispersed Li_2MnO_3-like domains would possess highly reversible oxygen redox and excellent structural stability, and exhibit superior cycling stability of high capacity. The findings provide new perspectives and concepts for designing high-energy Li-rich cathodes.

Keywords Co-free Li-rich layered oxides · Lithium-ion batteries · Li_2MnO_3-like domains · Electronic structure · Oxygen oxidation mechanism

Introduction

Cathode materials are a key component of lithium-ion batteries (LIBs) to determine electrochemical properties such as energy densities and rate performance [1–3]. Li-rich layered oxides (LLOs) have attracted much attention due to their high theoretical capacity of 250 mAh/g, which arises from the cumulative redox reactions of TM and oxygen ions [4–8]. It is widely accepted that the lattice oxygen with a linear Li–O–Li configuration provides extra specific capacity [9–13]. However, the irreversibility of oxygen redox makes LLOs undergo lattice oxygen release, structural degradation, and poor cycle performance [14, 15]. Consequent problems such as low initial Coulombic efficiency (ICE) and severe capacity/voltage fading seriously hinder commercial applications of LLOs [16–19].

LLOs structures with good reversibility of oxygen redox are being sought. It is widely accepted that LLOs consist of twin $LiTMO_2$ (TM = Mn, Co, Ni, etc.) and Li_2MnO_3-like domains [20, 21]. The key to controlling oxygen redox chemistry is to modulate the chemical environment of lattice oxygen with redox activity, that is, to modulate Li_2MnO_3-like domains. According to Pauling's rule [22], in the Mn-based LLOs, the coordination configuration OLi_4Mn_2 with Mn^{4+} is stable, making aggregated Li_2MnO_3-like domains popular [23, 24]. Recent researches have demonstrated that the large-sized and aggregated Li_2MnO_3-like domain would cause irreversible TM migration and oxygen release [25–27]. Cho's group found that the weak Mn–O covalency promoted excessive oxidation of oxygen ions and chemical irreversibility [25, 28]. Liu discovered that oxygen redox reversibility and cation migration could be suppressed by constructing Li_2ZrO_3

✉ Guixiao Jia
guixiao.jia@163.com

[1] Key Laboratory of Green Extraction and Efficient Utilization of Light Rare-Earth Resources, School of Materials and Metallurgy, Inner Mongolia University of Science and Technology, Baotou 014010, People's Republic of China

slabs into Li_2MnO_3-like domains [29]. Yu's study found that the 3:7 component with the least Li_2MnO_3-like component among $xLi_2MnO_3{\cdot}yLiMn_{0.42}Ni_{0.42}Co_{0.16}O_2$ ($x{:}y = 3{:}7$, 5:5, 7:3) had the best electrochemical performance and the higher reversibility of oxygen redox [12]. Bruce found that the oxidized oxygen ions in the $Na_{0.75}[Li_{0.25}Mn_{0.75}]O_2$ and $Li_{1.2}Ni_{0.13}Co_{0.13}Mn_{0.54}O_2$ with a honeycomb superstructure cannot be reduced and a large voltage hysteresis occurred, while the oxidization of lattice oxygen ions for systems with a band superstructure had good reversibility [30, 31]. Sun found that the aggregated Li_2MnO_3-like domains can lead to irreversible TM migration and oxygen release, while the dispersed Li_2MnO_3-like domains have inhibitory effects on TM migration and oxygen release [13]. Therefore, to control the size of Li_2MnO_3-like domains would be an effective strategy to improve the electrochemical performance of LLOs.

In our recent work, we demonstrated a highly stable layered $Li_{1.2}Ni_{0.2}Mn_{0.6}O_2$ LLOs with dispersed small-sized Li_2MnO_3-like domains by tuning the oxygen partial pressure during high-temperature calcination [32]. Our work revealed that $ONiMn^{4+}Mn^{3+}Li_3$ coordination configurations stabilized the Li-rich Li-Ni-Mn–O structure with small-sized Li_2MnO_3-like domains [32]. The small-sized Li_2MnO_3-like domains suppressed the O-release and enhanced the reversibility of oxygen redox and cycling performance by a special oxidation mechanism [32].

In LLO materials, high Ni content can contribute to the high capacity. Though LLO materials with the high Ni content have been a hot research topic now, the mixed arrangement of Li/Ni is still a problem to influence the cycle performance [33–36]. Layered Li-rich Li-Co–Ni-Mn–O LLOs are often used as one of the most promising cathode materials for the next generation battery because of their high capacity [37, 38]. However, the cost of Co element is expensive. Therefore, to develop Co-free cathode materials for LIBs is being pursued. Fe resources are rich in the earth. Its electronic structure is similar to other TM elements such as Co and Ni in manganese-based cathode materials and the contribution of Fe to the capacity is similar to that of Co in the terms of redox pairs [39, 40]. Previous studies have shown that Fe-substitution can suppress the oxygen release and improve the electrochemical properties [39–45]. Of course, these performances were also affected by compositions of the electrolyte and electrode–electrolyte interphases and so on [46, 47].

Therefore, the work selects a cobalt-free Li-rich layered material, $Li_{29}Fe_3Ni_3Mn_{13}O_{48}$(LFNMO), as the research object. Two models with dispersed Li_2MnO_3-like domains (D-LFNMO) and aggregated Li_2MnO_3-like domains (A-LFNMO) are built to study the Fe function and the effect of Li_2MnO_3-like domain size on the oxidation process, structures, and structural stability. This is different with our previous work in which the influence of the Li_2MnO_3-like domain size on electrochemical performance was only studied [32]. Oxidation process of cations and anions and the oxidation mechanism are explored using density of state (DOS) and electric density. Additionally, the TM ions (particularly Mn^{4+}) migration in LLOs with different Li_2MnO_3-like domain distribution also needs to be explored, since it is directly related to irreversible structural transformations and lattice oxygen release [48–51]. Consequently, structural stability is completed by calculating oxygen release energies and migration energies of Mn^{4+} ions from the TM layer to the Li vacancies at the TM layer and the Li layer. The study would provide a solid theoretical basis for the design of Li-rich cathode materials for cobalt-free lithium-ion batteries with high specific capacity and structure stability.

Calculation method and model

All calculations were performed using the VASP (Vienna Ab-initio simulation package) program. The spin-polarized generalized-gradient approximation (GGA) method with the Perdew-Burke-Ernzerhof (PBE) exchange correlation function [52] was used to study the $Li_{29}Fe_3Ni_3Mn_{13}O_{48}$ system (C2/m space group, $\alpha = \gamma = 90°$, $\beta \neq 90°$, $a \neq b \neq c$) containing 96 atomic positions ($Li_{1.208}Fe_{0.125}Ni_{0.125}Mn_{0.542}O_2$ formula). The core electrons were represented by the projector-augmented wave (PAW) potentials [53], and the valence electrons Li $2s^1$, Fe $3d^74s^1$, Ni $3d^84s^2$, Mn $3d^64s^1$, and O $2s^22p^4$ were expanded at a plane wave with the cutoff energy of 500 eV. Considering that the system contains the TM element with high angular quanta, we used the GGA + U method proposed by Dudarev et al. [54]. The included parameters U and J are not set separately, and only the difference value $U - J$ is meaningful. Therefore, we simplified the parameters to U, and U values of Fe, Ni, and Mn were 4.9 eV, 6.0 eV, and 4.9 eV, respectively, similar to our previous work [55]. The energy and force convergence criteria were set to 10^{-4} eV and 0.02 eV/Å, respectively. Ion and unit cell relaxations and the electronic structures were performed on the 96-atom-position model using a $2 \times 1 \times 4$ and $4 \times 2 \times 8$ Monkhorst–Pack (MP) k-points, respectively. Various possible ferromagnetic (FM) and antiferromagnetic (AFM) structures are considered. Calculations show that the most stable magnetic structure of $Li_{29}Fe_3Ni_3Mn_{13}O_{48}$ is AFM, see Fig. 1(a) and (b).

According to Pauling's rule [22], in the Mn-based LLOs, the coordination configuration OLi_4Mn_2 with Mn^{4+} is stable, making aggregated Li_2MnO_3-like domains popular [23, 24]. Recently, we have successfully synthesized layered Li-Ni-Mn–O LLOs with dispersed small-sized and aggregated Li_2MnO_3-like domains by tuning the oxygen partial pressure during high-temperature calcination, respectively, named A-LNMO and D-LNMO [32]. The average grain size of Li_2MnO_3-like

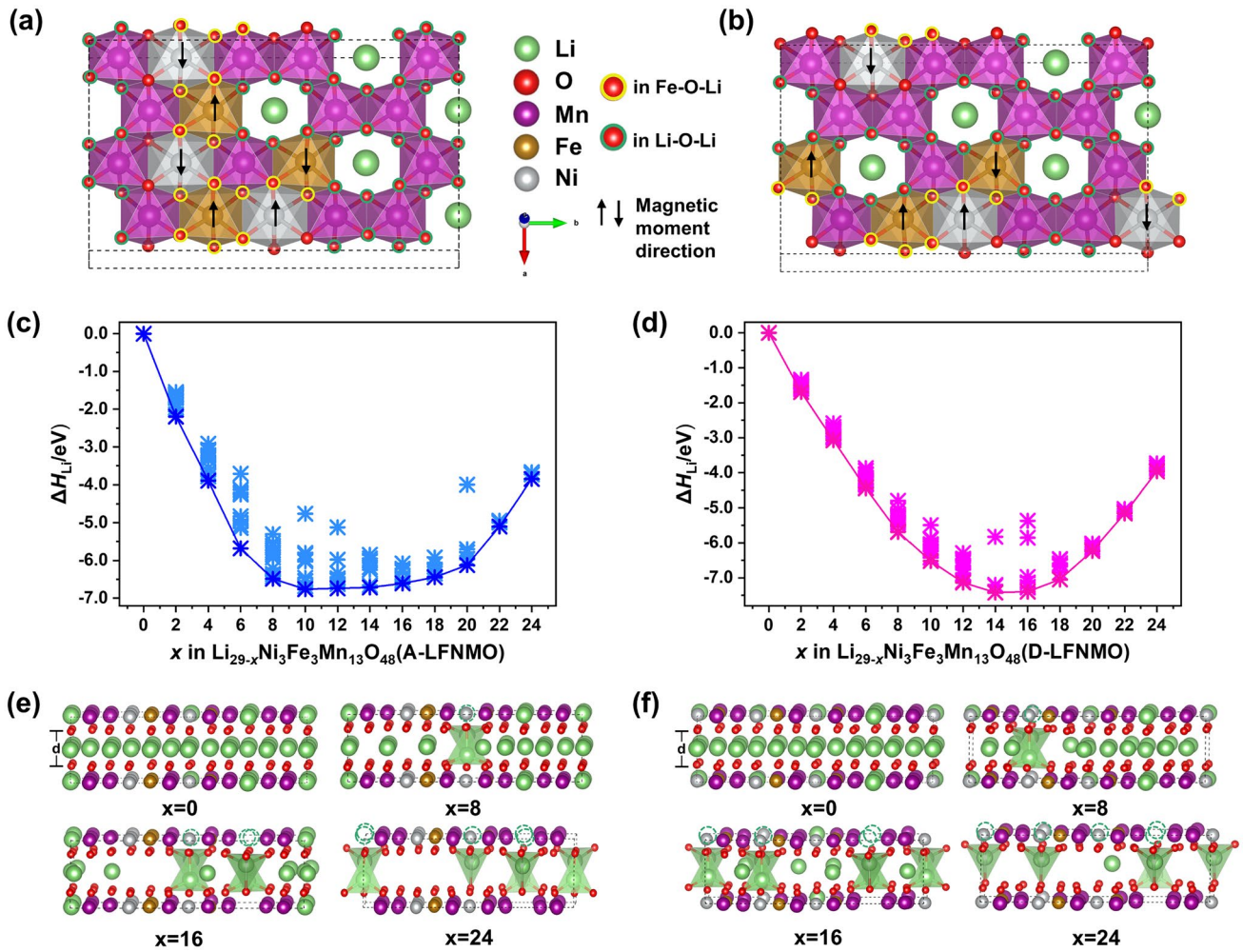

Fig. 1 A-LFNMO (**a**) and D-LFNMO (**b**) models of $Li_{29}Fe_3Ni_3Mn_{13}O_{48}$. The ΔH_{Li} of A-LFNMO (**c**) and D-LFNMO (**d**) as x in $Li_{29-x}Fe_3Ni_3Mn_{13}O_{48}$. The stable de-lithiation structures of A-LFNMO (**e**) and D-LFNMO (**f**) as x in $Li_{29-x}Fe_3Ni_3Mn_{13}O_{48}$

domains is 23.57 nm for D-LNMO, which is almost half that of A-LNMO (56.25 nm) [32]. D-LNMO possesses highly reversible oxygen redox and exceptional structural stability, exhibiting superior cycling stability of high capacity [32]. DFT calculation [32] selects Li-rich aggregated and dispersed models with 5 Å×9 Å×5 Å to simulate the LLOs with dispersed small-sized and aggregated Li_2MnO_3-like domains and well understands the experimental result in the terms of atomic and electronic structures. Therefore, this work employs a similar model to explore the effect of Li_2MnO_3-like domain size and Fe on the structural stability and oxidization. Herein, a cobalt-free Li-rich layered $Li_{29}Fe_3Ni_3Mn_{13}O_{48}$ with dispersed Li_2MnO_3-like domains (D-LFNMO) and aggregated Li_2MnO_3-like domains (A-LFNMO) is designed, see Fig. 1. In A-LFNMO and D-LFNMO, all possible structures with various atomic occupations are considered, and structures with the lowest energies are shown in Fig. 1(a) and (b), respectively. Ni likely occupies the rich-Li site in layered Li_2MnO_3 structures and Fe preferably occupies the Mn site in layered Li_2MnO_3 structures. The calculation finds that the energy difference between A-LFNMO and D-LFNMO structure with the lowest energies is 0.245 meV/fu (slight smaller than electron energy of 26 meV at the room temperature), namely, they can both exist in the synthetic compounds. In addition, we have found that the interfacial O ions between twin Li_2MnO_3-like and $LiTMO_2$ domains were easily triggered to participate into charge compensation [32].

In order to evaluate the structural stability of the $Li_{29-x}Fe_3Ni_3Mn_{13}O_{48}$ ($0 \le x \le 24$) system during charging, the ΔH_{Li} was calculated and the corresponding formula was followed:

$$\begin{aligned}\Delta H_{Li} = {} & E\left(Li_{29-x}Fe_3Ni_3Mn_{13}O_{48}\right) \\ & - \frac{x}{29}E\left(Fe_3Ni_3Mn_{13}O_{48}\right) \\ & - \left(1 - \frac{x}{29}\right)E\left(Li_{29}Fe_3Ni_3Mn_{13}O_{48}\right)\end{aligned} \quad (1)$$

where $E(Li_{29}Fe_3Ni_3Mn_{13}O_{48})$ and $E(Fe_3Ni_3Mn_{13}O_{48})$ were total energies of the $Li_{29}Fe_3Ni_3Mn_{13}O_{48}$ systems with all and no Li^+ ions, respectively. $E(Li_{29-x}Fe_3Ni_3Mn_{13}O_{48})$ was the total energy of the $Li_{29-x}Fe_3Ni_3Mn_{13}O_{48}$ system.

Instability of lattice oxygen in LLOs from aggregated Li_2MnO_3-like domains causes the irreversibility of oxygen redox and consequent structural damage and severe capacity/voltage fading. Herein, the enthalpy changes ΔH_O of the $Li_{29-x}Fe_3Ni_3Mn_{13}O_{48}$ ($0 \le x \le 24$) expressing the O–release was calculated and the corresponding formula was as followed:

$$\Delta H_O = E\left(Li_{29-x}Fe_3Ni_3Mn_{13}O_{47}\right) + 1/2E(O_2) - E\left(Li_{29-x}Fe_3Ni_3Mn_{13}O_{48}\right) \quad (2)$$

where $E(Li_{29-x}Fe_3Ni_3Mn_{13}O_{48})$ and $E(Li_{29-x}Fe_3Ni_3Mn_{13}O_{47})$ were the total energies of $Li_{29-x}Fe_3Ni_3Mn_{13}O_{48}$ systems without and with one O vacancy, respectively. $E(O_2)$ was the energy of the O_2 molecule. In addition, the average redox potential V_{ave} of $Li_{29-x}Fe_3Ni_3Mn_{13}O_{48}$ as de-lithiation amount x was calculated, and Eq. (3) was as follows:

$$V_{ave}(x1 \le x \le x2) = -\frac{E\left(Li_{29-x1}Fe_3Ni_3Mn_{13}O_{48}\right) - E\left(Li_{29-x2}Fe_3Ni_3Mn_{13}O_{48}\right) - (x2-x1)E(Li)}{(x2-x1)e} \quad (3)$$

where $E(Li)$ was the energy of one Li atom and $E(Li_{29-x1}Fe_3Ni_3Mn_{13}O_{48})$ and $E(Li_{29-x2}Fe_3Ni_3Mn_{13}O_{48})$ were the total energies of the $Li_{29-x}Fe_3Ni_3Mn_{13}O_{48}$ system as de-lithiation amount x is $x1$ and $x2$, respectively.

Bruce found that the oxidized O^{2-} ions on charging retained in the $Na_{0.75}[Li_{0.25}Mn_{0.75}]O_2$ and $Li_{1.2}Ni_{0.13}Co_{0.13}Mn_{0.54}O_2$ bulk through the in-plane migration of Mn^{4+} ions to form a local TM-O_2 structure [30, 31]. In addition, the out-plane migration of Mn^{4+} ions to the Li vacancy at the Li layer may happen and transform the layered structure to the spinel structure [56]. These structural transformations are irreversible, leading to the capacity/voltage fading [30, 31]. Therefore, in-plane and out-plane migrations of Mn^{4+} ions to Li vacancies are investigated by a climbing image nudged elastic band (CI–NEB) algorithm.

Results and discussion

Structure and energy evolutions of A-LFNMO and D-LFNMO during de-lithiation

Total energies of various possible de-lithiation structures for A-LFNMO and D-LFNMO are calculated as a criterion, see Fig. 1(c) and (d). Several most stable de-lithiation structures as examples are shown in Fig. 1(e) and (f). Calculations show that the Li-rich removal at the TM layer is often accompanied by the formation of LiO_4 tetrahedrons such as the structures with two tetrahedrons at $x = 8$, 16, and 24. The structural evolutions during the de-lithiation often are related with structural instability and the irreversibility of oxygen redox. Therefore, herein, the unit cell parameters, the O–O layer spacing (d) between the TMO_2 layers, the volume change before and after de-lithiation (ΔV), and Ni–O, Fe–O, and O–O bond lengths as the de-lithiation amount x in $Li_{29-x}Fe_3Ni_3Mn_{13}O_{48}$ are given, see Table 1 and Fig. 2.

The evolution rules of the unit cell parameters and the O–O layer spacing d of A-LFNMO are similar to D-LFNMO. With the increase of the de-lithiation amount x, the lattice constant a remains invariable, the lattice constant b slowly decreases, the lattice constant c gradually increases, the angle β first decreases and then increases, and the O–O layer spacing d shows a whole increase trend due to the coulomb repulsion of oxygen ions

Table 1 The cell parameters, O–O layer spacing (d), volume change (ΔV), and average de-lithiation potential (V_{ave}) of A-LFNMO and D-LFNMO (values in brackets are calculations of D-LFNMO)

x	a(Å)	b(Å)	c(Å)	β(°)	d(Å)	ΔV(%)	V_{ave}(V)*
0	5.05(5.05)	8.72(8.72)	5.09(5.09)	109.50(109.66)	2.77(2.77)	0.00(0.00)	–
2	5.03(5.06)	8.74(8.71)	5.09(5.11)	109.15(109.75)	2.81(2.82)	0.06(0.16)	3.41(3.67)
4	5.03(5.04)	8.71(8.71)	5.11(5.12)	109.13(109.45)	2.84(2.86)	0.03(0.33)	3.66(3.83)
6	5.04(5.04)	8.67(8.69)	5.13(5.16)	109.44(109.30)	2.88(2.92)	0.02(0.84)	3.62(3.84)
8	5.03(5.02)	8.66(8.68)	5.14(5.15)	109.72(109.51)	2.91(2.93)	−0.25(0.18)	4.11(3.89)
10	5.03(5.01)	8.63(8.66)	5.17(5.20)	110.08(109.88)	2.95(2.99)	−0.10(0.36)	4.37(4.10)
12	5.01(5.00)	8.64(8.63)	5.19(5.30)	110.50(111.56)	2.99(3.08)	−0.35(0.88)	4.52(4.21)
14	4.99(5.00)	8.64(8.62)	5.23(5.34)	110.66(112.33)	3.03(3.12)	−0.02(0.59)	4.52(4.38)
16	5.03(4.99)	8.61(8.61)	5.23(5.33)	110.77(112.55)	3.04(3.10)	−0.20(0.03)	4.57(4.53)
18	5.00(4.99)	8.60(8.59)	5.28(5.32)	111.67(112.32)	3.08(3.09)	−0.14(−0.21)	4.59(4.69)
20	5.00(4.98)	8.57(8.59)	5.30(5.36)	112.65(113.02)	3.09(3.14)	−0.70(−0.17)	4.67(4.92)
24	4.98(4.97)	8.60(8.59)	5.19(5.22)	108.17(108.08)	3.06(3.10)	0.02(−0.23)	5.14(5.12)

*This is the calculated value based on the Eq. (3) subtracting the escaping energy of one electron from the most stable Li surface

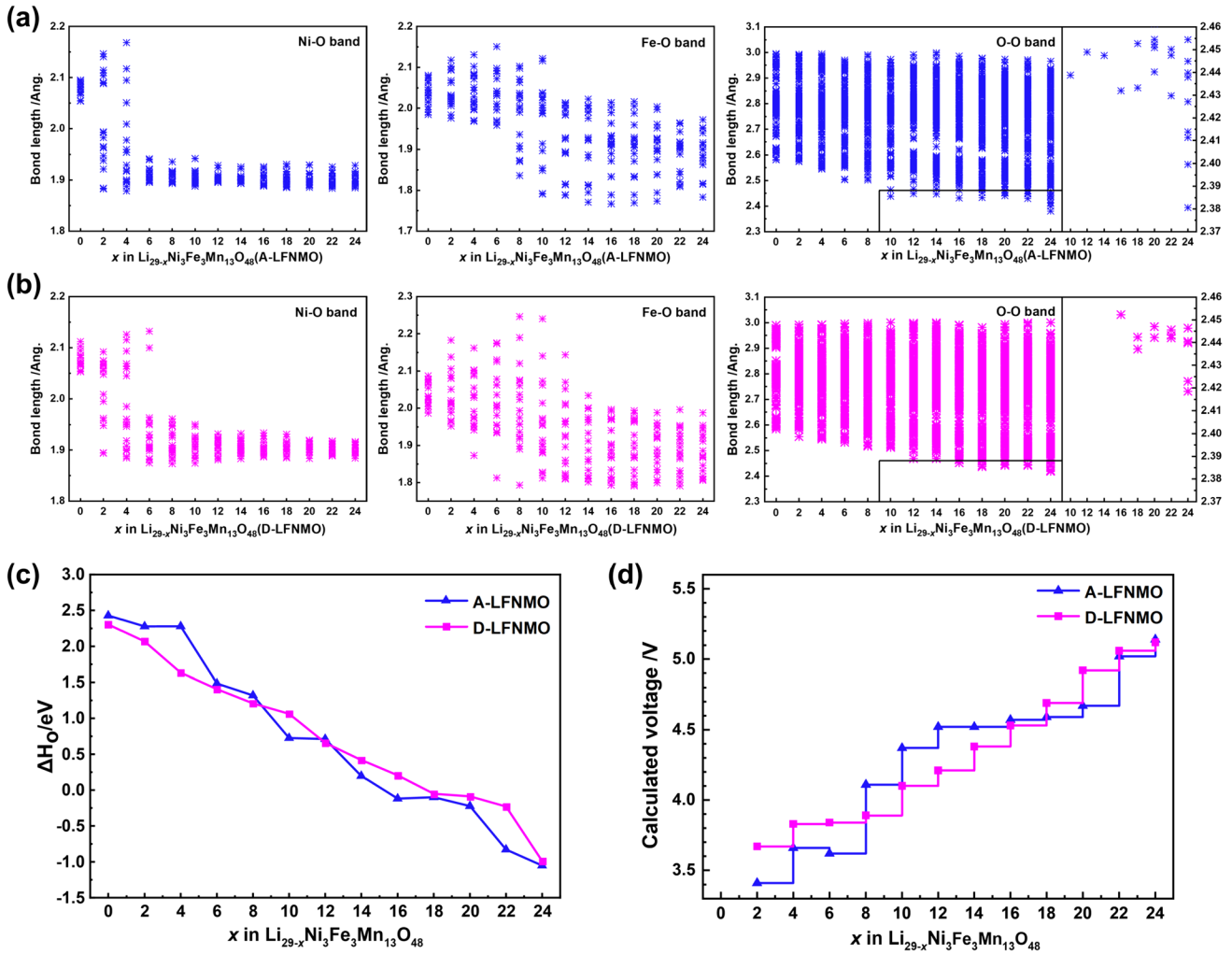

Fig. 2 Variations of the Ni–O, Fe–O, and O–O bond lengths in A-LFNMO (**a**) and D-LFNMO (**b**). Oxygen release enthalpy ΔH_O (**c**) and average de-lithiation potential V_{ave} (**d**) of A-LFNMO and D-LFNMO

between two TMO_2 layers, as shown in Table 1. These results are similar to our previous research finding on other Li-rich Li-Fe–Ni-Mn–O composition [55]. Regardless of D-LFNMO and A-LFNMO, the ΔV values are small and the largest value is only 0.88%. The ΔV values of D-LFNMO are larger than those of A-LFNMO due to larger d between the TMO_2 layers, see Table 1. The d changes are related to oxidization characteristic of lattice oxygen ions. More interfacial lattice O^{2-} ions in D-LFNMO participate into the oxidization (more interfacial O^{2-} ions in D-LFNMO [13], see the part on *Oxidation Process and Mechanism*); thus, the oxidization degree of every oxidized O^{2-} ions in D-LFNMO is slighter than that in A-LFNMO. Consequently, the Coulomb repulsion in D-LFNMO is larger than that in A-LFNMO, leading to larger d between the TMO_2 layers.

All the Ni–O, Fe–O and O–O bond lengths of every de-lithiation structures for A-LFNMO and D-LFNMO are listed. Their changes are related to the oxidation of Ni^{2+}, Fe^{3+}, and O^{2-}. For instance, when one or two among three Ni are oxidized, there are various Ni–O bond lengths, including shortened bonds due to Ni^{2+} ions toward Ni^{3+} or Ni^{4+} ions and elongated bonds to maintain the structures, well reflected in Fig. 2. The distribution range of Ni–O bond lengths first becomes wider and last converges to the shorter bonds till all Ni^{2+} ions are oxidized to Ni^{4+} at $x = 6$ for A-LFNMO and at $x = 8$ for D-LFNMO. Fe–O bond lengths become short due to charge compensation of Fe^{3+} ions after finishing oxidization of Ni^{2+} ions, and the distribution range is wide. Last, shortened O–O bond lengths appear due to the oxidization of oxygen ions, and shortened O–O bonds are concentrated on A-LFNMO, which is explained by their different oxidation characteristic of oxygen ions. This would maybe bring out their different stability of lattice oxygen.

To estimate the stability of lattice oxygen, O-release enthalpy ΔH_O with the de-lithiation amount x in $Li_{29-x}Fe_3Ni_3Mn_{13}O_{48}$ is calculated, shown in Fig. 2(c). The ΔH_O in D-LFNMO is higher than that in A-LFNMO

when the oxidization of lattice oxygen starts at $x > 9$ in $Li_{29-x}Fe_3Ni_3Mn_{13}O_{48}$. The higher ΔH_O means that the release of the lattice oxygen ions is suppressed, which would maybe improve the redox reversibility of the lattice oxygen ions in D-LFNMO, due to the different oxidation characteristic of oxygen with A-LFNMO. More interfacial O^{2-} ions in D-LFNMO participate in the oxidation (the detailed sees the next part and Sun's work [13]), that is, the dispersed Li_2MnO_3-like domains would provide the better reversibility of the oxygen redox. In addition, the oxidation process is divided into two parts, one is the oxidation of Ni^{2+} and Fe^{3+}, corresponding to redox pairs Ni^{2+}/Ni^{4+} and Fe^{3+}/Fe^{4+}(x=0–12 for A-LFNMO and x=0–10 for D-LFNMO), and another is the oxidation of lattice oxygen ($x \geq 8$ for A-LFNMO and $x \geq 10$ for D-LFNMO), shown in Fig. 2(d) and Table 1.

Oxidation process and mechanism of A-LFNMO and D-LFNMO during de-lithiation

Densities of states (DOS) and partial DOS (PDOS), which directly reflect the electronic structure changes during de-lithiation, are calculated to study the evolutions of electronic structures of D-LFNMO and A-LFNMO as the de-lithiation, see Fig. 3. For Ni, at x=0, the spin-up and spin-down states

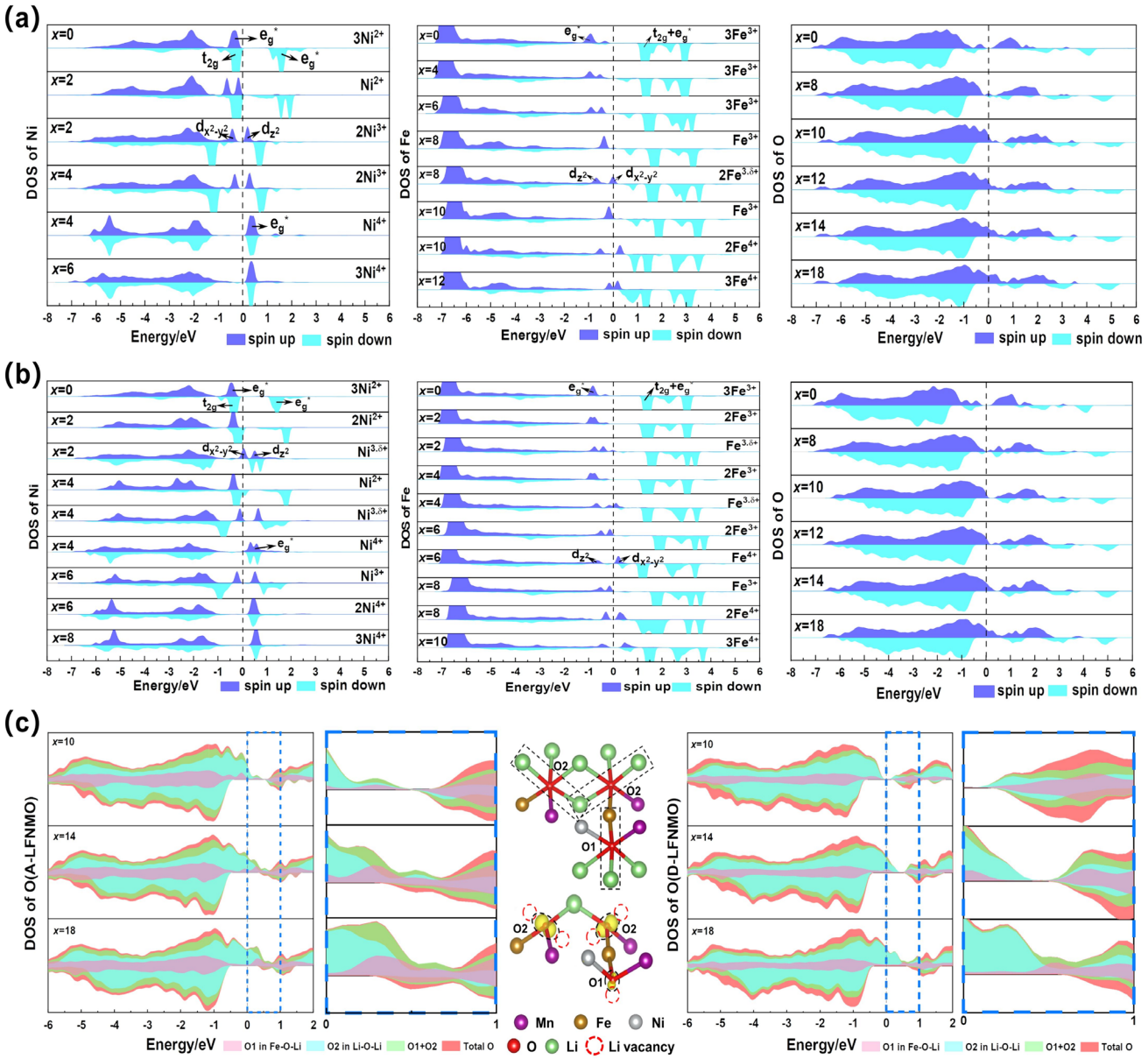

Fig. 3 DOS evolutions of Ni, Fe, and total O for A-LFNMO (**a**) and D-LFNMO (**b**) and the compared DOS for A-LFNMO and D-LFNMO (**c**) of O1 in the linear Fe–O-Li configuration, O2 in the linear Li–O-Li configuration, their sum and total O as the de-lithiation amount x in $Li_{29-x}Fe_3Ni_3Mn_{13}O_{48}$. Fermi level is set to 0 eV

of t_{2g} and the spin-up state of e_g^* occupy electrons, and the spin-down state of e_g^* is empty, indicating that the chemical valence of Ni is + 2, that is, Ni^{2+} $(t_{2g})^6(e_g^*)^2$. When de-lithiation starts, the spin-up d_z^2 for Ni loses electrons, that is, Ni^{2+} ions are oxidized to Ni^{3+}. As the de-lithiation goes forward, more spin-up d_z^2 loses electrons until the e_g^* state of Ni^{2+} ions become empty, namely all Ni^{2+} ions are oxidized to Ni^{4+} ions. DOS for Fe and O does not pass the Fermi level, that is, they are not oxidized. For Fe, at $x = 0$, all the spin-up states of t_{2g} and e_g^* are occupied, and all the spin-down states are empty, indicating that Fe is + 3 valence with the $(t_{2g})^3(e_g^*)^2$ configuration. During the de-lithiation, more $d_{x^2-y^2}$ of Fe becomes empty, indicating that Fe^{3+} ions are oxidized to + 4. Total state of lattice oxygen ions in D–LFNMO to exceed the Fermi level is later than that in A–LFNMO, and D–LFNMO happens at $x = 10$ and A–LFNMO happens at $x = 8$. This is confirmed by different initial oxidization potential V_{ave} of O in A–LFNMO and D–LFNMO, see Fig. 2(d) and Table 1.

In all, A–LFNMO and D–LFNMO have a similar charge compensation process during the de-lithiation process: Ni^{2+} is first oxidized to Ni^{4+}, then Fe^{3+} is oxidized to Fe^{4+}, last lattice oxygen participates into charge compensation, see Fig. 3(a) and (b). These results are similar to our previous

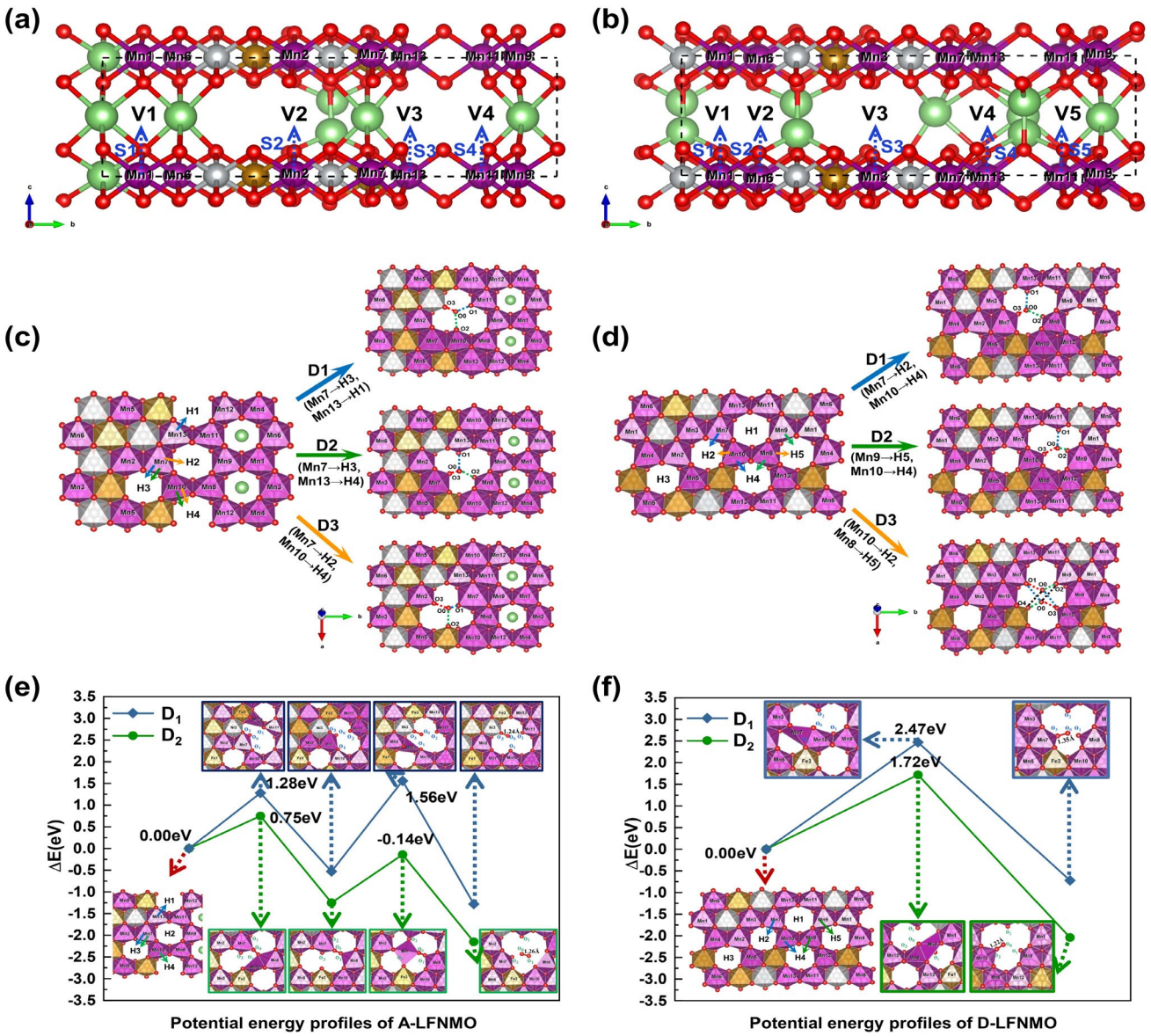

Fig. 4 The out-plane (**a**, **b**) and in-plane (**c**, **d**) migration path diagram of Mn^{4+} ions and their migration structures and energies of A-LFNMO (**e**) and D-LFNMO (**f**) ((**a**), (**c**), (**e**), at $x = 18$ in A-LFNMO; (**b**), (**d**), (**f**), at $x = 20$ in D-LFNMO). The out-plane migration paths: S1, S2, S3, S4, and S5; the in-plane migration paths: D1, D2, and D3. In product structures of the in-plane migration, the dotted lines are possible formed O–O dimer by one isolated O0 and its adjacent O1, O2, O3, or O4

research finding on other Li-rich Li-Fe–Ni-Mn–O composition [55]. As $x > 9$, oxygen begins to participate in charge compensation due to their states pass the Fermi level, see Fig. 3(a) and (b). At the energy range of 0–1.0 eV corresponding to the oxidization of lattice oxygen, we find that the lattice oxygen ions participated into charge compensation are O1 in the linear Fe–O-Li configuration, O2 in a linear Li–O-Li configuration and other O, samples at $x = 10,14$, and 18 as examples are presented, see Fig. 3(c). The DOS for other de-lithiation amount has a similar rule. O in $OTMFeLi_4$ (TM = Mn, Ni), not only in linear Fe–O-Li configuration but also in a linear Li–O-Li configuration, is named O2, because the 2p orbital of these oxidized O^{2-} ions is along a linear Li–O-Li direction, the unpaired O2p electron orbital direction with higher energy level, see Fig. 3(c). The amount of O1 in the linear Fe–O-Li configuration for A–LFNMO and D–LFNMO is the same, so they have the same contribution to the charge compensation in A–LFNMO and D–LFNMO if they have the same coordination environment. In fact, more OTM_2FeLi_3(TM = Mn, Ni, Fe) coordination configurations in A–LFNMO (Fig. 1(a)) make more O1 participate into charge compensation, see Fig. 3(c). Based on Sun's work that dispersed and aggregated Li_2MnO_3-like domains interfacial O between Li_2MnO_3-like and $LiTMO_2$ domains participated into the charge compensation [13], it is reasonably believed that the other lattice oxygen ions oxidized are interfacial O between Li_2MnO_3-like and $LiTMO_2$ domains. It is seen from Fig. 3(c) that D–LFNMO has more interfacial O between Li_2MnO_3-like and $LiTMO_2$ domains and less O1 in the linear Fe–O-Li configuration. Therefore, it can be concluded that the dispersion of Li_2MnO_3-like domains is more important to trigger more lattice oxygen ions to participate into charge compensation and the doping of Fe has a certain function.

Migration of Mn^{4+} ions of A-LFNMO and D-LFNMO during de-lithiation

Excessive oxidation of lattice oxygen ions makes LLOs unstable and brings out the structural transition and sequent capacity/voltage fading during cycling [48–51]. It has been found that the structural transformations such as Mn^{4+} ion migration to in-plane (forming the local TM–O_2 structure) [30, 31] or out-plane Li–vacancy (forming the spinel structure) are irreversible, affecting the cycle performances of LLOs. Therefore, the migration structures and energies of Mn^{4+} ions are explored, see Fig. 4. The lattice oxygen ions at $x = 16$ in A-LFNMO and $x = 18$ in D-LFNMO start to

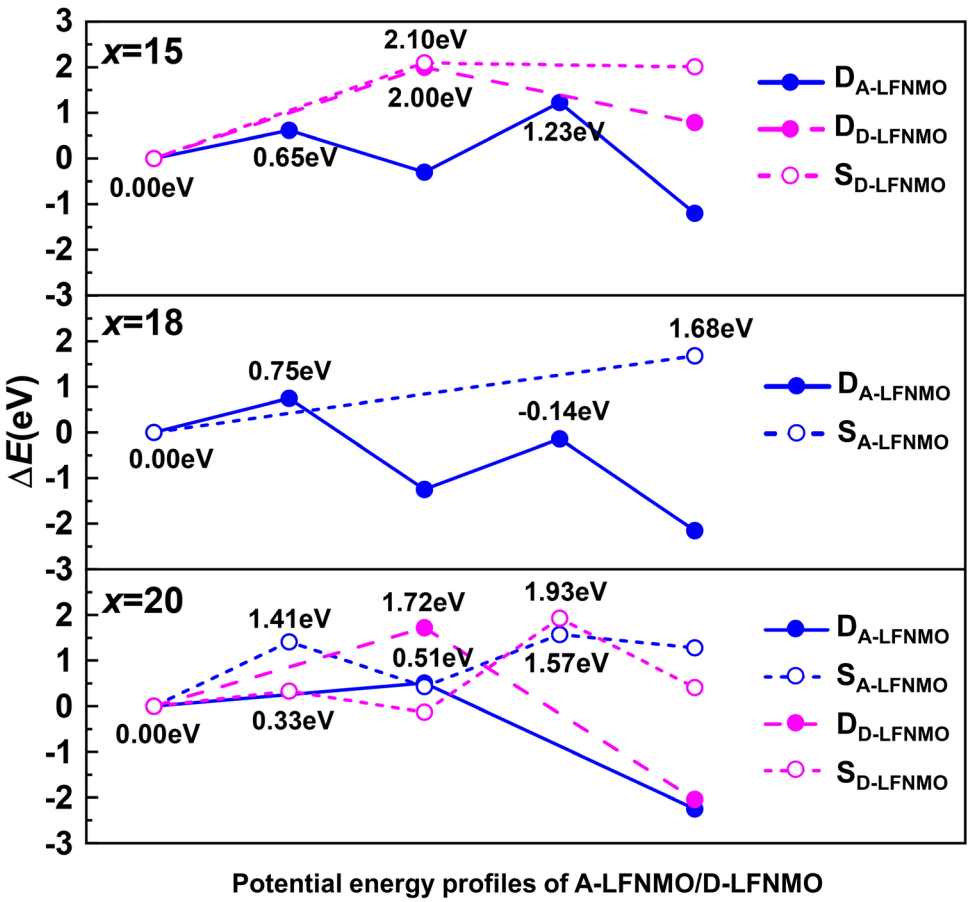

Fig. 5 Comparison of various migration energies of A-LFNMO and D-LFNMO. $D_{A\text{-}LFNMO}$ and $D_{D\text{-}LFNMO}$ or $S_{A\text{-}LFNMO}$ and $S_{D\text{-}LFNMO}$ are in-plane or out-plane migration of A-LFNMO and D-LFNMO, respectively

become unstable, so the migration energy, intermediate state, and transition state structures of Mn^{4+} ions around the de-lithiation amount $x = 16$ and $x = 18$ are considered.

As examples with $x = 18$ in A-LFNMO and $x = 20$ in D-LFNMO are used, it is found that the more stable migration product structures correspond to lower migration energies, shown in Fig. 4(e) and (f). Therefore, the migration paths with the most stable product structures are further investigated to simplify the calculations. Considering the calculation time, the sample at the deep de-lithiation amount $x = 20$ as an in-plane ($D_{A\text{-}LFNMO}$ and $D_{A\text{-}LFNMO}$) and out-plane ($S_{A\text{-}LFNMO}$ and $S_{A\text{-}LFNMO}$) migration example for A-LFNMO and D-LFNMO to completely studied. Figure 5 shows that the in-plane migration energies of D-LFNMO are all higher than those of A-LFNMO and migration energies of Mn^{4+} ions reduce with the de-lithiation amount x. For example, when $x = 15$, the in-plane migration energy of Mn^{4+} ions for D-LFNMO is 2.00 eV, larger than that for A-LFNMO (1.23 eV), and the in-plane migration energies of Mn^{4+} ions for A-LFNMO at $x = 15$, 18, and 20 are, respectively, 1.23 eV, 0.75 eV, and 0.51 eV. The small value of 0.51 eV indicates that the migration product with the local TM-O_2 structure would be easily formed. The out-plane migration energies of Mn^{4+} ions for A-LFNMO at $x = 18$ and 20 are, respectively, 1.68 eV and 1.57 eV, respectively larger than those of in-plane migration energies of 0.75 eV and 0.51 eV, showing that the out-plane migration is difficult. In all, the in-plane migration of Mn^{4+} ions is inclined to happen in A-LFNMO and regardless of A–LFNMO and D–LFNMO; the out-plane migration of Mn^{4+} ions is difficult because of large migration energies. These results indicate that the dispersed Li_2MnO_3-like domains suppress the in-plane migration of Mn^{4+} ions to form the local TM-O_2 structure, stabilizing the structures and consequently the improved the reversibility of the oxygen redox and cycle performances of LLOs.

Conclusion

In conclusion, de-lithiation structures, structural stability, and oxidization mechanism of lattice oxygen ions for Co-free LLOs with dispersed Li_2MnO_3-like domains (D–LFNMO) and aggregated Li_2MnO_3-like domains (A–LFNMO) are studied. Besides O^{2-} ions in the linear Li–O-Li configuration, the Fe-doping and especially dispersed Li_2MnO_3-like domains trigger more lattice oxygen ions, avoiding the peroxidation of lattice oxygen. During deep de-lithiation states, the oxygen release enthalpies of D–LFNMO are higher than those of A-LFNMO. At $x = 20$, the in-plane migration energy of Mn^{4+} ions with 0.51 eV for A–LFNMO shows that the irreversible migration product with the local TM-O_2 structure would be easily formed, vs. 1.72 eV, the large in-plane migration energy of Mn^{4+} ions for D–LFNMO. In addition, the large out-plane migration energies of Mn^{4+} ions (the largest migration energies at $x = 20$ are 1.41 eV for A–LFNMO and 1.93 eV for D–LFNMO) show that the out-plane migrations of Mn^{4+} ions would be difficult. In all, the in-plane migration of Mn^{4+} ions is inclined to happen in A-LFNMO and the out-plane migration of Mn^{4+} ions is difficult, regardless of A–LFNMO and D–LFNMO. D-LFNMO with the dispersion of Li_2MnO_3-like domains would stabilize the structures and improve cycle performance by suppressing the migration of Mn^{4+} ions and the oxygen release. This work would provide new insights and feasible strategies for developing high-performance Li-rich cathodes for advanced LIBs.

Funding The authors appreciate the financial support from the project of Inner Mongolia Natural Science Foundation (2021MS02003), the National Natural Science Foundation of China (Grant Nos. 52262039), and Inner Mongolia Basic Research Foundation.

Declarations

Competing interests The authors declare no competing interests.

References

1. Xu Q, Li X, Sari HM, Li W, Liu W, Hao Y, Qin J, Cao B, Xiao W, Xu Y, Wei Y, Kou L, Tian Z, Le S, Zhang C, Sun X (2020) Surface engineering of $LiNi_{0.8}Mn_{0.1}Co_{0.1}O_2$ towards boosting lithium storage bimetallic oxides versus monometallic oxides. Nano Energy 77:105034
2. Liu W, Li X, Xiong D, Hao Y, Li J, Kou H, Yan B, Li D, Lu S, Koo A, Adair K, Sun X (2018) Significantly improving cycling performance of cathodes in lithium-ion batteries: the effect of Al_2O_3 and $LiAlO_2$ coatings on $LiNi_{0.6}Co_{0.2}Mn_{0.2}O_2$. Nano Energy 44:111–120
3. Lv H, Li C, Zhao Z, Wu B, Mu D (2021) A review: Modification strategies of nickel-rich layer structure cathode (Ni≥0.8) materials for lithium-ion power batteries. J Energy Chem 60:435–450
4. Whittingham MS (2004) Lithium batteries and cathode materials. Chem Rev 104(10):4271–4302
5. Liu J, Bao Z, Cui Y, Dufek E, Goodenough J, Khalifah P, Li Q, Liaw BY, Liu P, Manthiram A, Meng Y, Subramanian V, Toney M, Viswanathan V, Whittingham M, Xiao J, Xu W, Yang J, Yang X-Q, Zhang J-G (2019) Pathways for practical high-energy long-cycling lithium metal batteries. Nat Energy 4(3):180–186
6. He W, Guo W, Wu H, Lin L, Liu Q, Han X, Xie Q, Liu P, Zheng H, Wang L, Yu X, Peng D-L (2021) Challenges and recent advances in high capacity Li-Rich cathode materials for high energy density lithium-ion batteries. Adv Mater 33(50):2005937
7. Rozier P, Tarascon JM (2015) Review—Li-rich layered oxide cathodes for next-generation Li-ion batteries: chances and challenges. J Electrochem Soc 162(14):A2490
8. Li B, Rousse G, Zhang L, Avdeev M, Deschamps M, Abakumov AM, Tarascon J-M (2023) Constructing, "Li-rich Ni-rich" oxide cathodes for high-energy-density Li-ion batteries. Energy Environ Sci 16(3):1210–1222

9. Kang S, Choi D, Lee H, Choi B, Kang Y-M (2023) A mechanistic insight into the oxygen redox of Li-rich layered cathodes and their related electronic/atomic behaviors upon cycling. Adv Mater 35(43):2211965
10. Seo D-H, Lee J, Urban A, Malik R, Kang S, Ceder G (2016) The structural and chemical origin of the oxygen redox activity in layered and cation-disordered Li-excess cathode materials. Nat Chem 8(7):692–697
11. Yin Z, Zhu H, Huang Y, Luo D, Ren Y, Lan S, Liu Q (2022) Approaching a stable oxygen redox reaction in lithium-rich cathode materials: structural perspectives from mechanism to optimization. J Mater Chem A 10(37):19387–19411
12. Yu H, So Y-G, Ren Y, Wu T, Guo G, Xiao R, Lu J, Li H, Yang Y, Zhou H, Wang R, Amine K, Ikuhara Y (2018) Temperature-sensitive structure evolution of lithium-manganese-rich layered oxides for lithium-ion batteries. J Am Chem Soc 140(45):15279–15289
13. Zhuo H, Peng H, Xiao B, Wang Z, Liu X, Li Z, Li G, Bai X, Wang L, Huang X, Wu J, Quan W, Wang J, Zhuang W, Sun X (2023) Atomic-scale revealing the structure distribution between $LiMO_2$ and Li_2MnO_3 in Li-rich and Mn-based oxide cathode materials. Adv Energy Mater 13(14):2203354
14. Sun G, Yu F-D, Zhao C, Yu R, Farnum S, Shao G, Sun X, Wang Z-B (2021) Decoupling the voltage hysteresis of Li-rich cathodes: electrochemical monitoring, modulation anionic redox chemistry and theoretical verifying. Adv Funct Mater 31(1):2002643
15. Zhou Y, Cui H, Qiu B, Xia Y, Yin C, Wan L, Shi Z, Liu Z (2021) Sufficient oxygen redox activation against voltage decay in Li-rich layered oxide cathode materials. ACS Materials Letters 3(4):433–441
16. Liu Y, Tang L, Wei H, Zhang X, He Z, Li Y, Zheng J (2019) Enhancement on structural stability of Ni-rich cathode materials by in-situ fabricating dual-modified layer for lithium-ion batteries. Nano Energy 65:104043
17. Song J, Ning F, Zuo Y, Li A, Wang H, Zhang K, Yang T, Yang Y, Gao C, Xiao W, Jiang Z, Chen T, Feng G, Xia D (2023) Entropy stabilization strategy for enhancing the local structural adaptability of Li-rich cathode materials. Adv Mater 35(7):e2208726
18. Zhang M, Li Z, Yu L, Kong D, Li Y, Cao B, Zhao W, Wen J, Pan F (2020) Enhanced long-term cyclability in Li-rich layered oxides by electrochemically constructing a $LixTM_{3-x}O_4$-type spinel shell. Nano Energy 77:105188
19. Zuo W, Luo M, Liu X, Wu J, Liu H, Li J, Winter M, Fu R, Yang W, Yang Y (2020) Li-rich cathodes for rechargeable Li-based batteries: reaction mechanisms and advanced characterization techniques. Energy Environ Sci 13(12):4450–4497
20. Liu T, Liu J, Li L, Yu L, Diao J, Zhou T, Li S, Dai A, Zhao W, Xu S, Ren Y, Wang L, Wu T, Qi R, Xiao Y, Zheng J, Cha W, Harder R, Robinson I, Wen J, Lu J, Pan F, Amine K (2022) Origin of structural degradation in Li-rich layered oxide cathode. Nature 606(7913):305–312
21. Yu H, Ishikawa R, So Y-G, Shibata N, Kudo T, Zhou H, Ikuhara Y (2013) Direct atomic-resolution observation of two phases in the $Li_{1.2}Mn_{0.567}Ni_{0.166}Co_{0.067}O_2$ cathode material for lithium-ion batteries. Angew Chem Int Ed 52(23):5969–5973
22. Pauling L (1929) The principles determining the structure of complex ionic crystals. J Am Chem Soc 51(4):1010–1026
23. Yin C, Wei Z, Zhang M, Qiu B, Zhou Y, Xiao Y, Zhou D, Yun L, Li C, Gu Q, Wen W, Li X, Wen X, Shi Z, He L, Shirley Meng Y, Liu Z (2021) Structural insights into composition design of Li-rich layered cathode materials for high-energy rechargeable battery. Mater Today 51:15–26
24. Liu S, Wang B, Zhang X, Zhao S, Zhang Z, Yu H (2021) Reviving the lithium-manganese-based layered oxide cathodes for lithium-ion batteries. Matter 4(5):1511–1527
25. Hwang J, Myeong S, Jin W, Jang H, Nam G, Yoon M, Kim SH, Joo SH, Kwak SK, Kim MG, Cho J (2020) Excess-Li localization triggers chemical irreversibility in Li- and Mn-rich layered oxides. Adv Mater 32(34):e2001944
26. Li Z, Li Y, Zhang M, Yin Z-W, Yin L, Xu S, Zuo C, Qi R, Xue H, Hu J, Cao B, Chu M, Zhao W, Ren Y, Xie L, Ren G, Pan F (2021) Modifying $Li@Mn_6$ superstructure units by Al substitution to enhance the long-cycle performance of Co-free Li-rich cathode. Adv Energy Mater 11(37):2101962
27. Song Y, Zhao X, Wang C, Bi H, Zhang J, Li S, Wang M, Che R (2017) Insight into the atomic structure of Li_2MnO_3 in Li-rich Mn-based cathode materials and the impact of its atomic arrangement on electrochemical performance. J Mater Chem A 5(22):11214–11223
28. Zhang C, Wei B, Wang M, Zhang D, Uchiyama T, Liang C, Chen L, Uchimoto Y, Zhang R, Wang P, Wei W (2022) Regulating oxygen covalent electron localization to enhance anionic redox reversibility of lithium-rich layered oxide cathodes. Energy Storage Materials 46:512–522
29. Zhang J, Zhang Q, Wong D, Zhang N, Ren G, Gu L, Schulz C, He L, Yu Y, Liu X (2021) Addressing voltage decay in Li-rich cathodes by broadening the gap between metallic and anionic bands. Nat Commun 12(1):3071
30. House RA, Maitra U, Pérez-Osorio MA, Lozano JG, Jin L, Somerville JW, Duda LC, Nag A, Walters A, Zhou K-J, Roberts MR, Bruce PG (2020) Superstructure control of first-cycle voltage hysteresis in oxygen-redox cathodes. Nature 577(7791):502–508
31. House RA, Rees GJ, Pérez-Osorio MA, Marie J-J, Boivin E, Robertson AW, Nag A, Garcia-Fernandez M, Zhou K-J, Bruce PG (2020) First-cycle voltage hysteresis in Li-rich 3d cathodes associated with molecular O_2 trapped in the bulk. Nat Energy 5(10):777–785
32. Li J, Li W, Zhang C, Han C, Chen X, Zhao H, Xu H, Jia G, Li Z, Li J, Zhang Y, Guo X, Gao F, Liu J, Qiu X (2023) Tuning Li_2MnO_3-like domain size and surface structure enables highly stabilized Li-rich layered oxide cathodes. ACS Nano 17(17):16827–16839
33. Ju P, Ben L, Li Y, Yu H, Zhao W, Chen Y, Zhu Y, Huang X (2023) Designer particle morphology to eliminate local strain accumulation in high-nickel layered cathode materials. ACS Energy Lett 8(9):3800–3810
34. Lin R, Bak S-M, Shin Y, Zhang R, Wang C, Kisslinger K, Ge M, Huang X, Shadike Z, Pattammattel A, Yan H, Chu Y, Wu J, Yang W, Whittingham MS, Xin HL, Yang X-Q (2021) Hierarchical nickel valence gradient stabilizes high-nickel content layered cathode materials. Nat Commun 12(1):2350
35. Yoon S, Park HG, Koo S, Hwang J, Lee Y, Park K, Kim D (2023) An in-depth understanding of chemomechanics in Ni-rich layered cathodes for lithium-ion batteries. J Alloy Compd 939:168531
36. Yu L, Liu T, Amine R, Wen J, Lu J, Amine K (2022) High nickel and no cobalt-the pursuit of next-generation layered oxide cathodes. ACS Appl Mater Interfaces 14(20):23056–23065
37. Chu B, Guo Y-J, Shi J-L, Yin Y-X, Huang T, Su H, Yu A, Guo Y-G, Li Y (2022) Cobalt in high-energy-density layered cathode materials for lithium-ion batteries. J Power Sources 544:231873
38. Shi Y, Kim K, Xing Y, Millonig A, Kim B, Wang L, Lee E, Harrison C, Yu T, Johnson DC, Lipson AL, Durham JL, Liu D, Fister TT, Yu L, Wen J (2020) Facile and scalable dry surface doping technique to enhance the electrochemical performance of $LiNi_{0.64}Mn_{0.2}Co_{0.16}O_2$ cathode materials. J Mater Chem A 8(38):19866–19872
39. Laisa CP, Nanda Kumar AK, Selva Chandrasekaran S, Murugan P, Lakshminarasimhan N, Govindaraj R, Ramesha K (2016) A comparative study on electrochemical cycling stability of lithium rich layered cathode materials $Li_{1.2}Ni_{0.13}M_{0.13}Mn_{0.54}O_2$ where M = Fe or Co. J Power Sources 324:462–474
40. Cheng X, Wei H, Hao W, Li H, Si H, An S, Zhu W, Jia G, Qiu X (2019) A cobalt-free $Li(Li_{0.16}Ni_{0.19}Fe_{0.18}Mn_{0.46})O_2$ cathode for

lithium-ion batteries with anionic redox reactions. ChemSusChem 12(6):1162–1168
41. Croy JR, Long BR, Balasubramanian M (2019) A path toward cobalt-free lithium-ion cathodes. J Power Sources 440:227113
42. Gao Y, Wang X, Ma J, Wang Z, Chen L (2015) Selecting substituent elements for Li-rich Mn-based cathode materials by density functional theory (DFT) calculations. Chem Mater 27(9):3456–3461
43. Liu W, Li J, Li W, Xu H, Zhang C, Qiu X (2020) Inhibition of transition metals dissolution in cobalt-free cathode with ultrathin robust interphase in concentrated electrolyte. Nat Commun 11(1):3629
44. Nakahara K, Tabuchi M, Kuroshima S, Toda A, Tanimoto K, Nakano K (2012) Drastically improved performances of graphite/$Li_{1.26}Mn_{0.52}Fe_{0.22}O_2$ cell with stepwise pre-cycling treatment that causes peroxide forming. J Electrochem Soc 159(9):A1398–A1404
45. Zhao T, Ji R, Yang H, Zhang Y, Sun X, Li Y, Li L, Chen R (2019) Distinctive electrochemical performance of novel Fe-based Li-rich cathode material prepared by molten salt method for lithium-ion batteries. J Energy Chem 33:37–45
46. Wu F, Li W, Chen L, Su Y, Bao L, Bao W, Yang Z, Wang J, Lu Y, Chen S (2020) Renovating the electrode-electrolyte interphase for layered lithium-& manganese-rich oxides. Energy Storage Materials 28:383–392
47. Dong J, Wu F, Zhao J, Shi Q, Lu Y, Li N, Cao D, Li W, Hao J, Yang X (2023) Multifunctional self-reconstructive cathode/electrolyte interphase layer for cobalt-free Li-rich layered oxide cathode. Energy Storage Materials 60:102798
48. Cai X, Zhang N, Ding H, Zhao D, Zhou J, Zhang J, Song L, Huang J, Li C, Li S (2023) Understanding the mechanism of performance difference when substituting Al for different transition metal ions in Li-rich Mn-based cathode materials. Acta Mater 258:119220
49. Eum D, Kim B, Kim SJ, Park H, Wu J, Cho S-P, Yoon G, Lee MH, Jung S-K, Yang W, Seong WM, Ku K, Tamwattana O, Park SK, Hwang I, Kang K (2020) Voltage decay and redox asymmetry mitigation by reversible cation migration in Lithium-rich layered oxide electrodes. Nat Mater 19(4):419–427
50. House RA, Marie J-J, Pérez-Osorio MA, Rees GJ, Boivin E, Bruce PG (2021) The role of O_2 in O-redox cathodes for Li-ion batteries. Nat Energy 6(8):781–789
51. Xiao B, Liu H, Chen N, Banis MN, Yu H, Liang J, Sun Q, Sham T-K, Li R, Cai M, Botton GA, Sun X (2020) Size-mediated recurring spinel sub-nanodomains in Li- and Mn-rich layered cathode materials. Angew Chem Int Ed 59(34):14313–14320
52. Kresse G, Furthmüller J (1996) Efficient iterative schemes for ab initio total-energy calculations using a plane-wave basis set. Phys Rev B Condens Matter 54(16):11169–11186
53. Tackett A, Holzwarth N, Matthews G (2001) A projector augmented wave (PAW) code for electronic structure calculations, Part II: pwpaw for periodic solids in a plane wave basis. Comput Phys Commun 135:348–376
54. Dudarev SL, Botton GA, Savrasov SY, Humphreys CJ, Sutton AP (1998) Electron-energy-loss spectra and the structural stability of nickel oxide: an LSDA+U study. Phys Rev B Condens Matter 57(3):1505–1509
55. Wei H, Cheng X, Fan H, Shan Q, An S, Qiu X, Jia G (2019) A cobalt-free $Li(Li_{0.17}Ni_{0.17}Fe_{0.17}Mn_{0.49})O_2$ cathode with more oxygen-involving charge compensation for lithium-ion batteries. ChemSusChem 12(11):2471–2479
56. Jo MR, Kim Y, Yang J, Jeong M, Song K, Kim Y-I, Lim J-M, Cho M, Shim J-H, Kim Y-M, Yoon W-S, Kang Y-M (2019) Triggered reversible phase transformation between layered and spinel structure in manganese-based layered compounds. Nat Commun 10(1):3385